Bull Eng Geol Environ (2016) 75:1157–1168
DOI 10.1007/s10064-016-0885-3

ORIGINAL PAPER

Effects of groundwater withdrawal on land subsidence in Kashan Plain, Iran

Akbar Ghazifard[1] · Ali Moslehi[1] · Homayon Safaei[1] · Mahasa Roostaei[2]

Received: 1 December 2015 / Accepted: 8 April 2016 / Published online: 22 April 2016

Abstract Kashan Plain is located in an arid area on the west side of central desert of Iran in north of Isfahan province. In recent decades, increasing population, industrial and agricultural developments in the region that require water withdrawal have resulted in the decline of groundwater and the occurrence of subsidence in this plain. Since 1991, earth fissures that have caused many damages to buildings, farmlands and roads have been observed in many parts of Kashan Plain. The lengths of some of these fissures are more than 2 km long. In this study, after determining the location and direction of fissures, the probable influential causes of earth fissuring were investigated. The results indicated that the main causes of this phenomenon are basically the decline of groundwater head, variation in sediment thickness due to bedrock anomalies and differential vertical compaction. In order to investigate the rate of land subsidence in the Kashan Plain, the Envisat ASAR data from 2003 to 2008 were used. The displacement maps were generated by InSAR time series analysis. The maximum rate of subsidence in this period was determined to be about 3.5 cm/year.

Keywords Land subsidence · Water withdrawal · InSAR · Kashan Plain

✉ Akbar Ghazifard
ghazifard@yahoo.com; ghazifar@sci.ui.ac.ir

[1] Department of Geology, Faculty of Sciences, University of Isfahan, Hezar Jarib Ave, Isfahan, Iran

[2] Geological Survey of Iran, Tehran, Iran

Introduction

Land subsidence is a gradual settling or sudden sinking of the earth surface associated with some horizontal displacements (Bates and Jackson 1980). The natural occurrence of this phenomenon is usually due to geological processes such as solubility, thawing of ice, vibration, gentle crustal movement and densification of deposits. Man-made related occurrences are due to mining activities, hydro compaction and withdrawal of oil, gas and groundwater (Waltham 1989; Bell 1999). In recent decades, groundwater withdrawal is becoming one of the most important causes of land subsidence and earth fissuring in many parts of the world, such as in Venice, Italy (Gambolati et al. 1974); Arizona, USA (Schumann and Cripe 1986); Mexico City, Mexico (Adrian et al. 1999); Hanoi, Vietnam (Trinh and fredlund 2000); Bangkok, Thailand (Phien-Wej et al. 2006) and Changzhou, China (Wang et al. 2009). The maximum recorded amounts of subsidence by excessive groundwater withdrawal were 9 m in Sanjoaquin valley in California, 9 m in Mexico City and 5.3 m in Santa Clara Valley of California (Waltham 1989). When ground water declines, the hydrostatic pressure also declines, and eventually leads to the reduction of pore water pressure and the gradual transfer of stress from the pore water to the granular structure (Bell 1999). As the grains carry this increased load, the fabric of the affected sediment may deform in order to adjust to the new stress condition. As a result, the sediment void ratio will decline, and the ground surface gradually subside (Bell 1999). There are several suggested mechanisms that explain how the earth fissures can be formed due to groundwater withdrawal. These mechanisms are differential vertical compaction (Feth 1951; Bouwer 1977; Jachens and Holzer 1979; Holzer and Pampeyan 1981; Jachens and Holzer

1982) and horizontal aquifer movements (Lofgren 1978; Helm 1994). Geological characteristics such as aquifer faults (Sheng et al. 2003; Kontogianni et al. 2007), bedrock ridge (Jachens and Holzer 1982; Slaff 1993) and heterogeneous aquifer (Sheng et al. 2003) are the most important factors that affect the differential vertical compaction.

There are a variety of methods available for monitoring land subsidence. They include vertical extensometers, leveling, baseline and repeated surveys of benchmarks using global positioning system (GPS) or conventional survey methods, and Interferometric synthetic aperture radar (InSAR) (Galloway and Burbey 2011). The InSAR technique is uniquely suited to monitor elastic and inelastic responses of aquifer systems to changes in groundwater levels and provide a new insight into the role of geological structures and lithological parameters in plain aquifers (Amelung et al. 1999; Hoffmann et al. 2001; Bell et al. 2002; Motagh et al. 2008). These methods provide an unsurpassed spatial sampling density (100 pixels/km^2), a competitive precision, and a useful observation cadence (1 month passage) (Massonnet and Feigl 1998). InSAR offers new capabilities to measure surface deformation caused by aquifer discharge and recharge at an unprecedented level of detail that was not previously possible, with techniques like GPS and leveling (Hoffmann et al. 2001; Bell et al. 2002; Schmidt and Burgmann 2003).

Regional land subsidence in Iran was reported for the first time in Rafsanjan Plain in 1967 (Mousavi et al. 2001). Since then, these phenomena have also been reported in other plains such as Tehran, Mashhad, Kerman, Yazd (Motagh et al. 2008).

Kashan Plain is one of the most important plains in Isfahan Province. In 1991, large earth fissures caused by subsidence appeared in southwest region of this plain. The earth fissures inflicted damages to 90 homes and many farmlands. Since then, the earth fissuring has spread in many parts of the plain and has caused further damages to buildings, farmlands and roads. Due to intense fissuring and subsidence-related adverse effects, a comprehensive study was needed to investigate the main causes of this phenomenon in Kashan Plain.

Area description

Kashan Plain is located at 205 km north of Isfahan Province and 240 km south of Tehran (51°5′E to 51°55′E and at 33°45′N to 34°23′N) (Fig. 1).

Geology

The geologic outcrops in the west and south of the Kashan Plain are a series of Cenozoic Plutonic and volcanic rocks (granite, rhyolite, andesite and andesite basalt) and a series of Mesozoic and Cenozoic sedimentary rocks (conglomerate, marl, limestone and shale). In the eastern portion of the study area, there is a series of interglacial Quaternary sand dunes (Fig. 2).

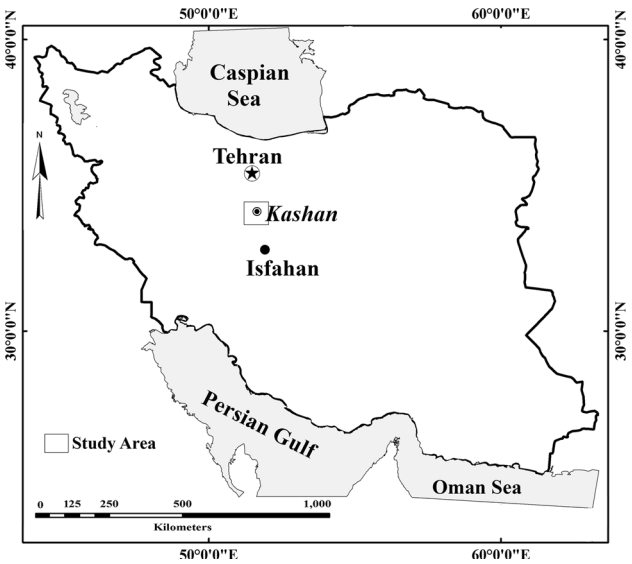

Fig. 1 Location of the study area

Hydrology

In the study area, the aquifer type is unconfined type and is composed of Quaternary alluvium, which are transported from the highlands to the west of Kashan and deposited on the Kashan Plain. In western and southern parts near the highlands, the sediments are mostly coarse grained and form into alluvial fans (Fig. 8). In north and northeast parts of the plain, the sediments are mostly fine grain silts and clays. According to the studies reported by Isfahan Department of Regional Water, the storativity coefficient in the study area is about 4 %, and the maximum coefficient of transmissivity is about 900 m^2/day around Ravand area while the minimum coefficient of transmissivity is about 100 m^2/day around Aran area. Kashan Plain is located in an arid area. The average annual precipitation is 138.4 mm, annual absolute maximum temperature is 48 °C and annual evaporation rate is 2379.7 mm. Because Kashan Plain is situated approximately north of Great Kavir (playa), there is lack of adequate precipitation or any perennial streams, groundwater is the main source of water supply and natural vegetation cover is very limited. The earliest deep well was drilled in 1956, in which the depth of groundwater was only 2 m from the surface, in the southeastern region of the plain. With increasing population and agricultural activities in recent decades, the number of drilled wells from 1965 to 2005 increased from 67 to 924,

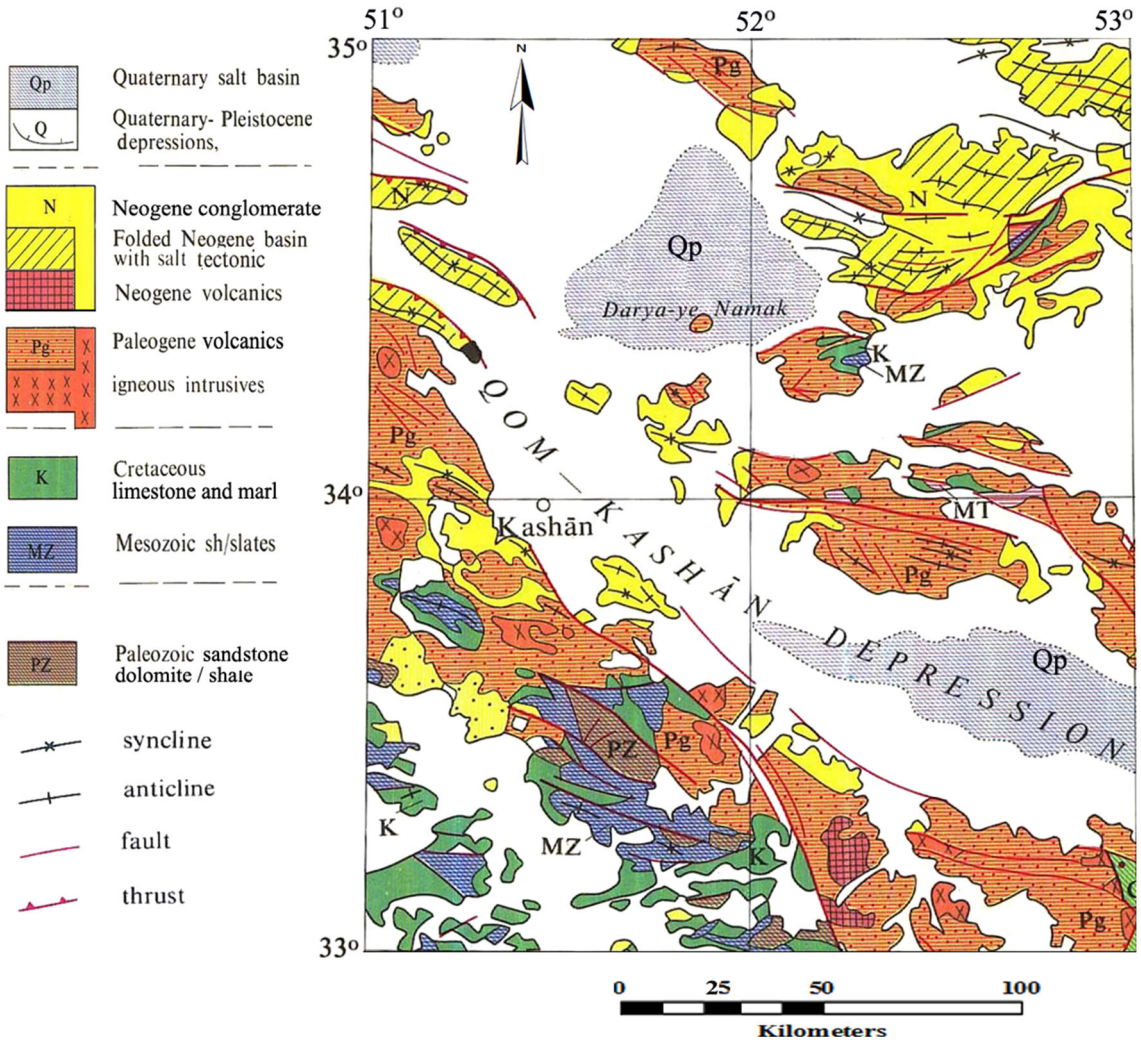

Fig. 2 Geological map of the study area (geological survey of Iran)

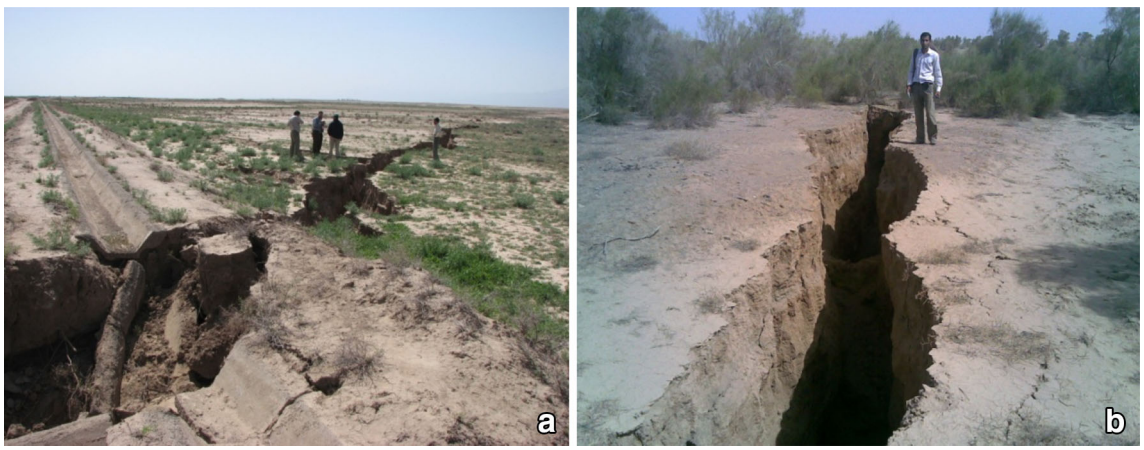

Fig. 3 Examples of surface fissures in Kashan Plain. **a** North of Ravand (about 1 km long and 1–2 m deep, fissure #1 on Fig. 14b); **b** East of Kashan City (2 km long and 2–3 m deep, fissure #2 on Fig. 14c)

respectively, which caused a considerable decline in groundwater head in the plain. As a result, most of the Qanats also dried up and the discharges of old wells were significantly reduced. Qanats are over 2000-year-old hand dug tunnels that are used to transfer water from highlands to villages and towns in lowlands for drinking and irrigation consumption. The total volume of water withdrawal from the aquifer in 2009 was about 282.5 million cubic meters, over 86 % of which was consumed in agricultural activities.

Materials and methods

In order to investigate the objectives of this study, the following methods were used.

First, the size, direction and location of about 400 of the fissures were measured using GPS. Because the geoelectrical method has significant ability to determine the thickness of alluvial deposits, depth and shape of the bedrocks, it was used in this study. The isopach map of alluvium thickness and bedrock topography was generated

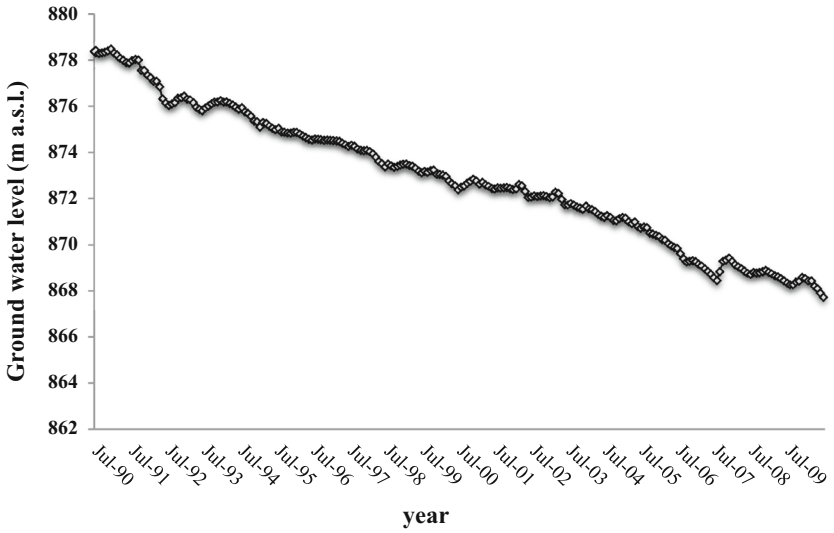

Fig. 4 Average decline of groundwater head, obtained from 65 available piezometers in Kashan Plain from 1990 to 2010

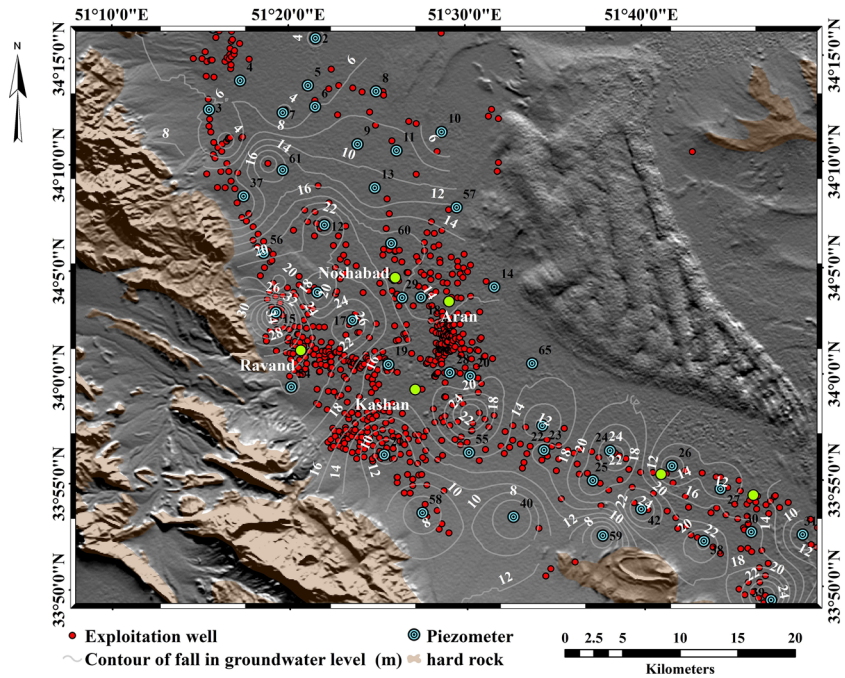

Fig. 5 Map of declined groundwater head in the study area (1990–2010), location of exploitation wells and 65 available piezometers in Kashan Plain (Base map is SRTM)

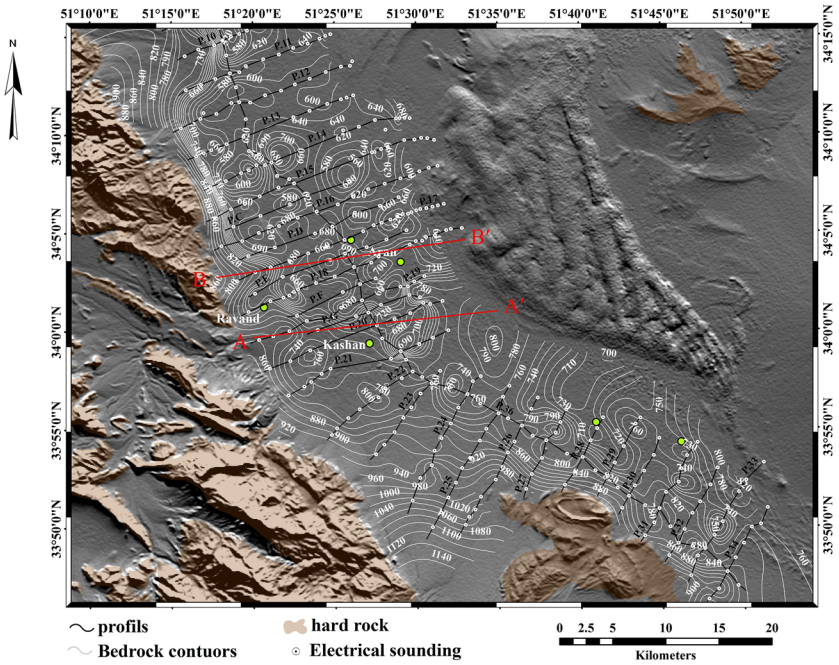

Fig. 6 Map of bedrock topography along with location of vertical electric sounding and geoelectric profiles in the study area. *AA′* and *BB′ lines* show the locations of lithological cross sections presented in Fig. 8 (Base map is SRTM)

by using a geoelectrical survey that was conducted with maximum length of 1500 m flow line and 396 vertical electric soundings in 42 profiles. Changes of the groundwater table were monitored with 65 available piezometers during a 20-year period, which permitted the evaluation of groundwater head decline.

In order to measure ground subsidence and its area of influence, the InSAR technique was used. This technique can help scientists to measure land deformation from space, and accurately map the spatially dense changes of surface displacements in the satellite's line of sight (Amelung et al. 1999). More precisely, it derives information from the interferograms, which are formed by phase differences between two high resolution SAR images, for the same area, obtained at slightly different positions (Saracin et al. 2014). Differential interferometric synthetic aperture radar (DInSAR) is a technique based on InSAR. It removes the topographic phase with an external digital elevation model (DEM), leaving the phase component related to land motion between the two images (Raucoules et al. 2007; Donglie et al. 2014). In addition, for detection of slow deformation over a long time span, other InSAR techniques have been developed. One of these techniques, which is referred to in this study, is a small baseline subset method (SBAS) used for creating time series of surface displacements from a set of interferograms (Berardino et al. 2002). In this method, interferograms with short spatial and temporal baselines are processed. In order to estimate the temporarily smooth Persistent Scatterers Interferometry (PSI), which performs an analysis of 'persistent scatterer', inversion on a pixel-by-pixel basis is carried out (Donglie et al. 2014). Another approach is Persistent Scatterers Interferometry (PSI), which performs an analysis of 'persistent scatterer' pixels on a succession of time-ordered images (Berardino et al. 2002; Donglie et al. 2014).

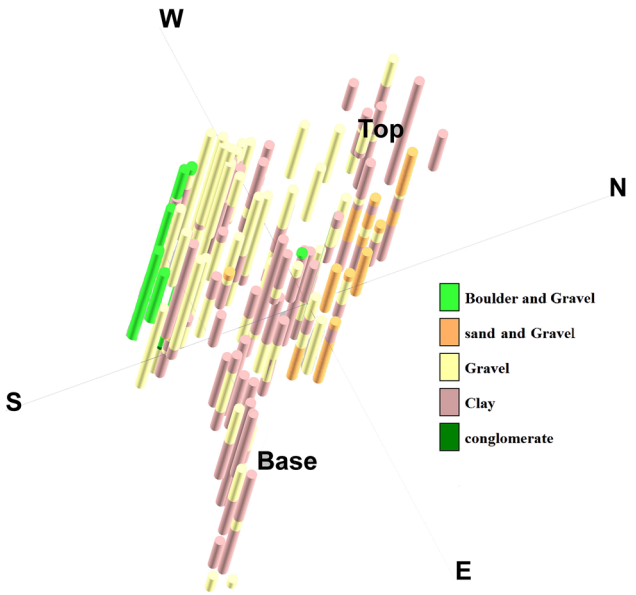

Fig. 7 Log of available piezometers used for cross section preparation

After designating the locations of fissures and subsidence zones, they were correlated with the location of fissures, the amount of water table decline, topography of bedrock and thickness of sediments. In order to correlate the thickness of compressible sediments (such as clay) and

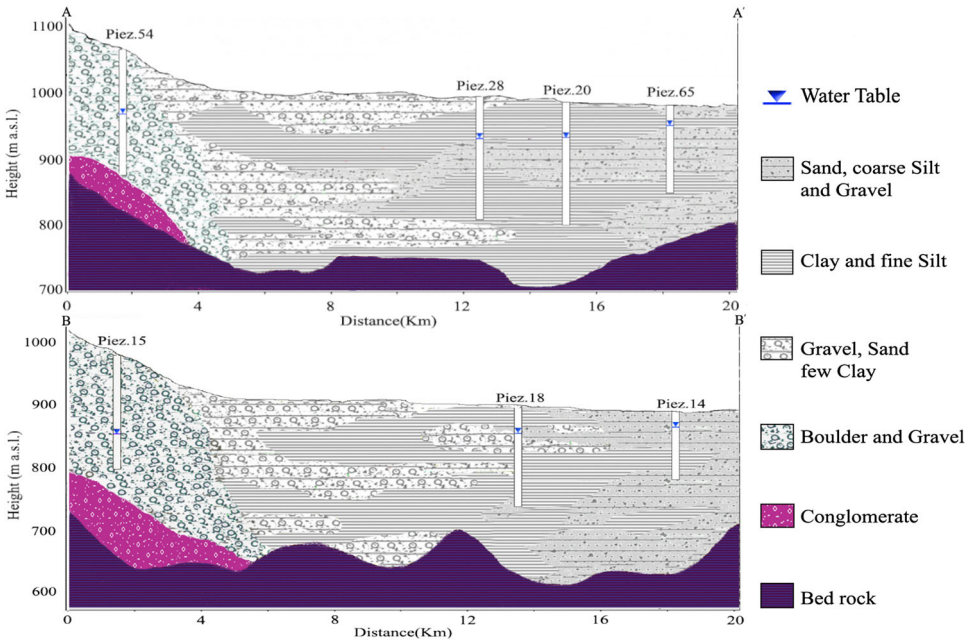

Fig. 8 Lithological cross sections prepared based on *AA′* (**a**) and *BB′* (**b**) *lines* designated on Kashan Plain map in Fig. 6

Table 1 List of nine Envisat Descending tracks 378 SAR scenes

No	Date	Day diff	Orbit number	Baseline diff (m)
1	2003.10.12	70	8448	−789
2	2004.06.13	315	11955	−542
3	2004.07.18	350	12456	−472
4	2004.10.31	385	12957	−82
5	2004.12.05	455	13959	−650
6	2005.04.24	490	14460	−489
7	2005.10.16	630	16464	−904
8	2005.11.20	805	18969	−320
9	2008.04.13	840	19470	−615

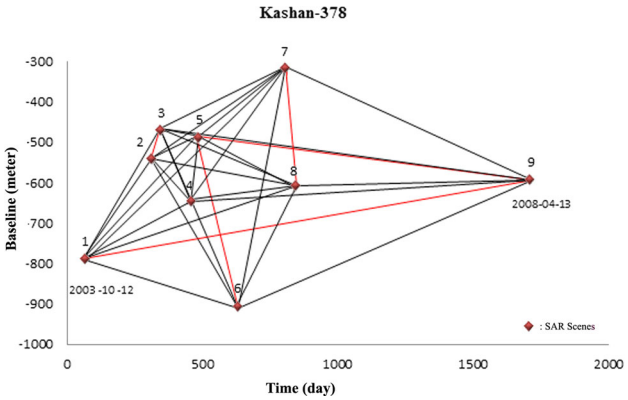

Fig. 9 Plot of 36 processed interferograms from nine SAR scenes (*Black lines* show processed interferograms from two SAR scenes that used for time series; for example, interferograms between SAR scenes 1 and 6. *Red lines* show processed Interferograms from two SAR scenes that were overwhelmed with atmospheric water vapor and orbital errors and have not been used for time series; for example, interferograms between SAR scenes 1 and 9)

subsidence zones, the borehole logs of 65 available piezometers and some exploitation wells were used.

Results and discussion

Field survey

The main natural features of land subsidence are the formation of fissures and cracks in the area. In fact, these features are the evidence of subsidence phenomenon (Fig. 3a, b).

After the situations of fissures on the ground were determined, they are overlaid on the map of the study area. The results indicate that: (1) fissures in central and northwestern part of the study area do not follow the specific trend; (2) the length of fissures varies from a few decimeters to several kilometers and (3) the shapes of fissures are different (straight, curved and polygonal) (Fig. 14b, c).

Decline in groundwater head

The decline in groundwater head is one of the most important causes of land subsidence worldwide. When discharge of an aquifer is significantly greater than its natural recharge, the aquifer generally experiences a great increase in effective stress and subsequent strain and deformation (Burbey 2002). Subsidence in Kashan Plain also experiences the same behavior. The obtained

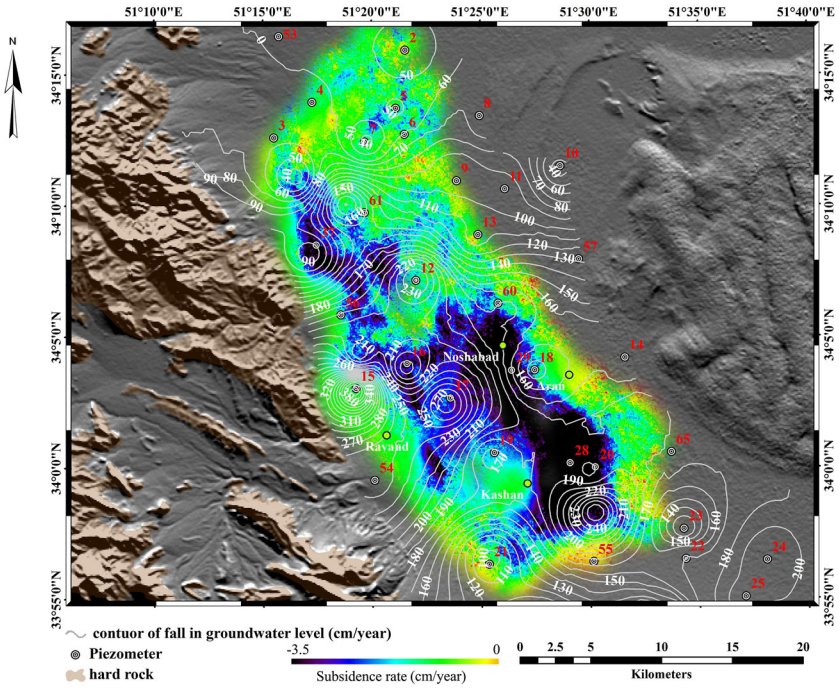

Fig. 10 Map of annual rate of subsidence, annual rate of decline in groundwater head and location of the available piezometers

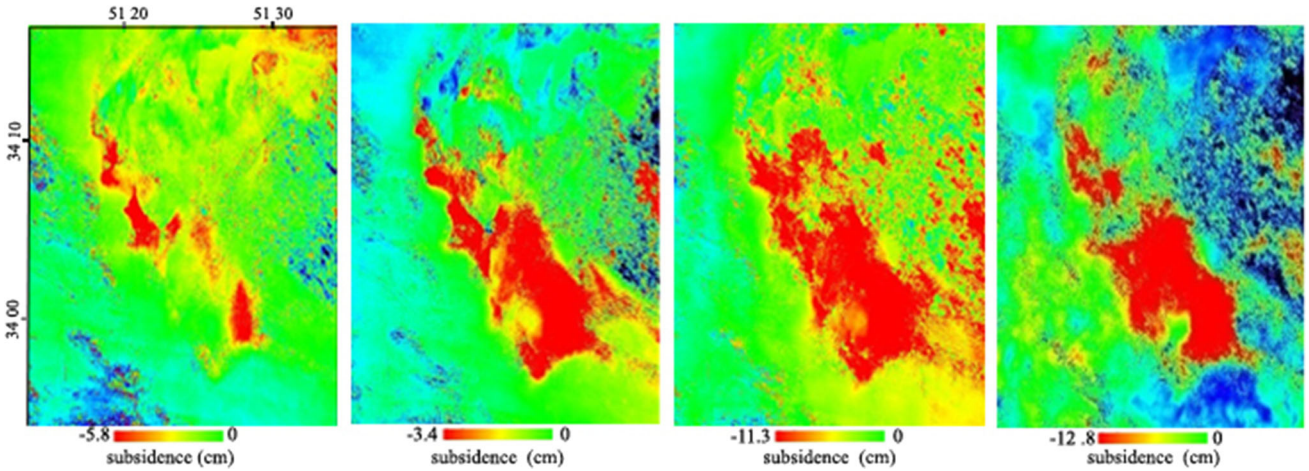

Fig. 11 Processed interferograms from four pairs of SAR scenes to correlate subsidence and fall in groundwater level from 2003 to 2008

hydrograph indicated that groundwater levels have been falling due to an increase in the number of deep wells and groundwater pumpage (Fig. 4). As shown, the maximum decline in groundwater head occurred in 1991 when the first earth fissures in Kashan Plain were observed. The average decline of groundwater head, obtained from 65 available piezometers from 1990 to 2010, is about 0.58 m/year (Fig. 4). The contour map of declined groundwater head from 1990 to 2010 was prepared based on 65 available piezometers (Fig. 5). According to this map, the maximum decline of groundwater head in the western region is approximately 40 m, while in the central region near the city of Kashan, it is about 24 m.

Bedrock anomaly and sediment thickness

By using vertical electric sounding and geoelectric profiles, the bedrock topography, and sediment thicknesses were determined. The results indicate that the sediment thicknesses vary from 40 to 340 m and the bedrock is neither flat nor characterized by uniform shapes. In some parts of the plain, the bedrock topography has a pinnacled shape (Fig. 6). In order to correlate the thickness of compressible sediments (such as clay and silt) with subsidence zones, the borehole logs of 65 available piezometers and some exploitation wells were prepared (Fig. 7), and from these logs two lithological cross sections (Fig. 8) were drawn

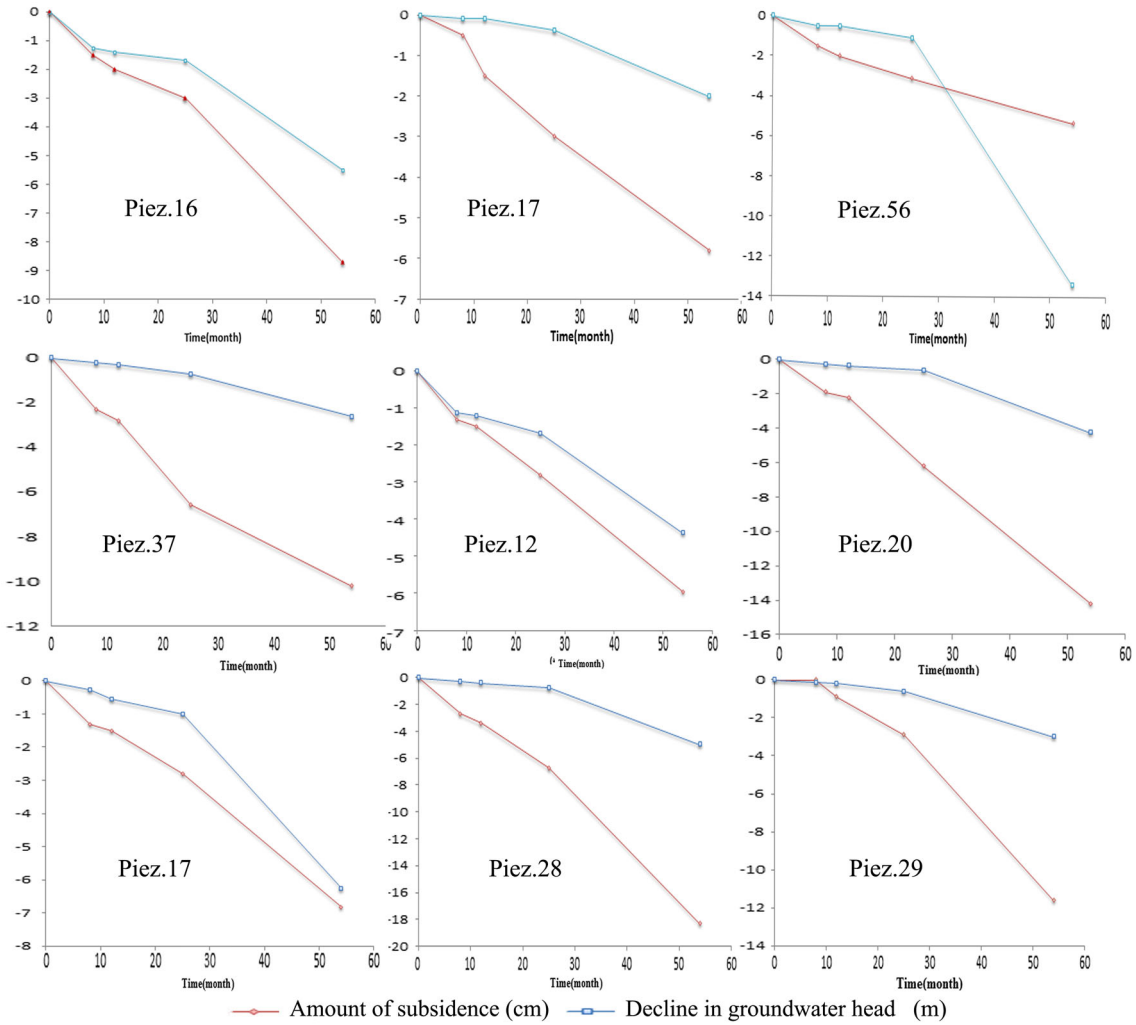

Fig. 12 Relation between decline in groundwater head and amount of subsidence from 12 October 2003 to 13 April 2008 (54 months)

based on AA′ and BB′ lines designated on Kashan Plain map in Fig. 6.

Radar interferometery and time series analysis (InSAR time series analysis)

In this study, nine Envisat SAR scenes of descending track 378 were sorted in chronological order (Table 1). The Single Look Complex (ASA_IMS_1p product) images were processed with Gamma software (Werner et al. 2000) using four pixels in the range direction and 20 pixels in the azimuth direction to give an interferogram pixel size of about 80 by 80 m on the ground. In order to remove the topographic effect and geocoding interferograms, the Shuttle Radar Topography Mission (SRTM) with the spatial resolution of 90 m was applied (Farr and Kobrick 2000).

An adaptive filter using a 32 by 32 pixel boxer smoothing window is performed to the data before unwrapping (Goldstein and Werner 1998). From 20 November 2005 to 13 April 2008, there were about 875 days to establish a temporal baseline. Because the spanning period from 2003 to 2008 for time series analysis is more important, the minimum cost flow (MCF) algorithm to unwrapping phase is applied. The results of the time series algorithms with SBAS (Berardino et al. 2002) from 31 out of 36 created interferograms and the five interferograms overwhelmed with atmospheric water vapor and orbital errors are shown in Fig. 9.

The best fitting plane in the far field is removed from each interferogram, and the interferograms are calibrated with respect to a high coherent pixel located in a non-deforming area. The reference image is selected to decrease the atmospheric effects on the time series. The maximum subsidence rate reveals roughly about 3.5 cm/year in the central part of the Kashan Plain (Fig. 10).

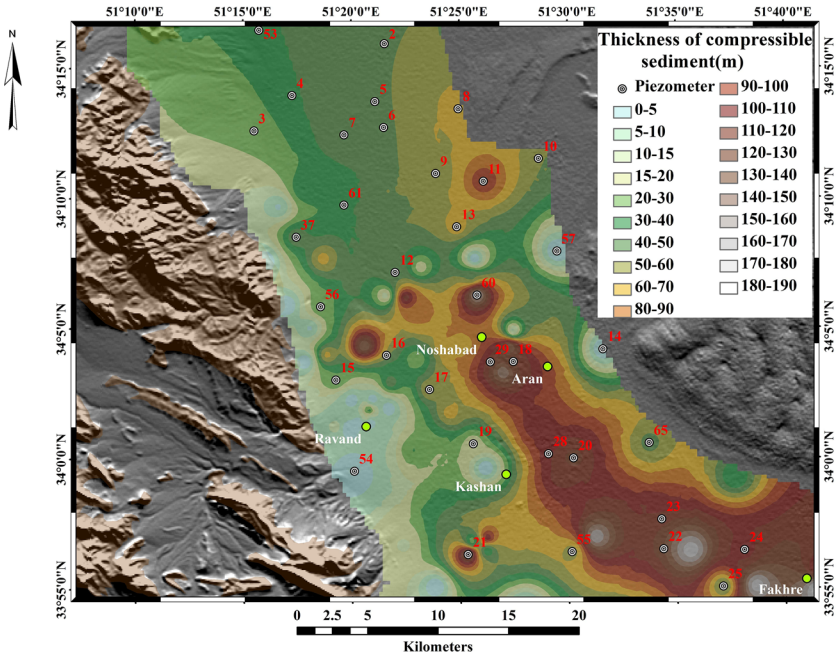

Fig. 13 Map of compressible sediment thickness

Relation between decline in groundwater head and subsidence area

In order to determine the relationship between the decline in groundwater head and subsidence area, the map of annual rate of subsidence and annual rate of decline in groundwater head was compared. The results show that the maximum annual subsidence occurred between the Kashan and Aran areas, nearly correlating with the maximum amount of annual decline in groundwater head (Fig. 10). Although the fall in groundwater level is high in the western part of the study area, the amount of subsidence is not significant. This phenomenon can be due to the presence of coarse grain sediments deposited by alluvial fans in this area.

Furthermore, decline in groundwater head and amount of subsidence are directly compared in nine locations from 2003 to 2008. To prepare an accurate data from the rate of decline in groundwater head, points near the available piezometers are selected. Then, the amount of subsidence for these points is calculated using InSAR. In this process, the data from five SAR scenes are used (SAR scenes 1, 2, 4, 8 and 9 from Table 1) and four interferograms are created (Fig. 11). More SAR scenes could be used for this process, but because of very little difference between some of these data, only the above SAR scenes were selected (Fig. 9).

The results of the above processes are presented in Fig. 12, which shows that the decline in groundwater head and the amount of annual subsidence are closely correlated. In graph number 28, located east of Kashan City, the amount of subsidence is 18.3 cm, whereas the decline in groundwater head is 4.95 m in 54 months. This means that for each 1 m of decline, about 3.7 cm of ground subsidence has occurred. In graph number 29, located south of Noshabad, the amount of subsidence is 11.6 cm for 3 m of decline in groundwater level, showing that the subsidence rate is about 3.8 cm for 1 m of decline in groundwater level. But in graph number 56, the decline in groundwater head is 13.3 m and the amount of subsidence is about 5.38 cm, which shows the rate of subsidence is about 0.4 cm for 1 m of decline in groundwater head. This lower rate is most likely due to presence of coarse grain sediments in the area (Fig. 13). These findings are similar with studies conducted by Ezquerro et al. (2014) and Herrera et al. (2009).

Relation between subsidence area, bedrock anomaly, sediment thickness and earth fissures

In order to investigate the relation between subsidence area, bedrock anomalies and sediment thickness, the map of annual subsidence rate is compared with thickness of sediments (Fig. 14a). The results indicate that the maximum subsidence is occurring east of Kashan, where bedrock is bowl-like and thickness of compressible sediment is high (Figs. 13, 14a). According to Boni et al. (2015), Herrera et al. (2009), Sheng et al. (2003) and Rojas et al. (2002), the maximum subsidence can occur where the sediment thickness and thickness of compressible sediment are greatest.

In this area, most of the fissures have also been formed at places with higher sediment thicknesses (Fig. 14b, c). In fact, changes in aquifer thickness as aquifer heterogeneity

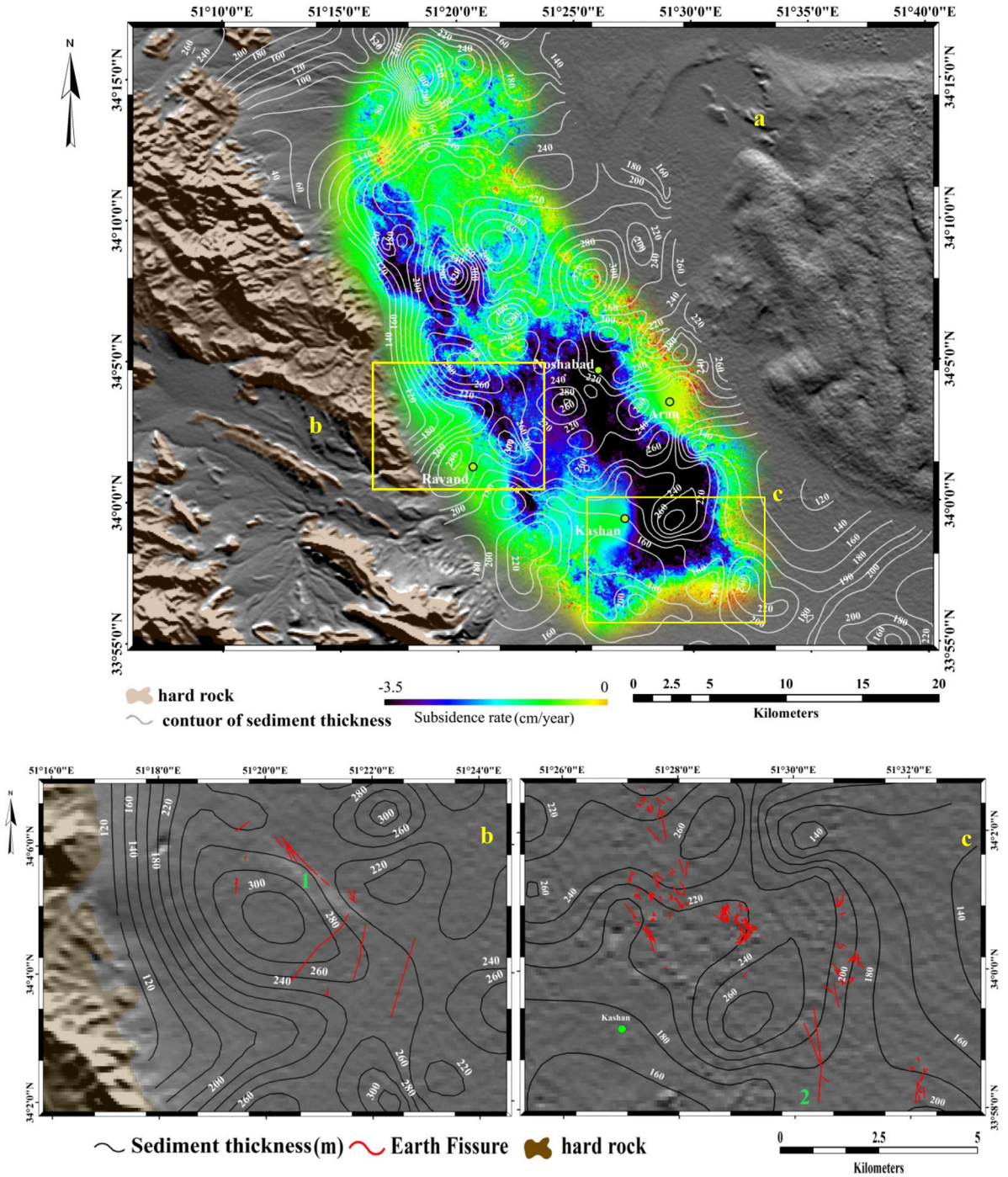

Fig. 14 **a** Map of annual rate of subsidence and sediment thickness; **b**, **c** location of earth fissures at the border of the subsidence bowl area with highest sediment thickness in Kashan Plain

is introduced can cause geometrical irregularity in the aquifer (Sheng et al. 2003; Slaff 1993; Freyre et al. 2003), in which the amount of the vertical compaction around geometrical irregularities will be different. According to Rojas et al. (2002), the maximum vertical displacement occurs at the center, and the maximum horizontal displacement occurs at the border of the bowl. Horizontal displacement generates tensile strains in the area in which earth fissures are formed (Fig. 15).

In order to show the relation between location of earth fissure and subsidence zone, 36 interferograms were selected for processing. The results of these processing are shown in Fig. 15a (from 12 Oct 2003 to 13 Jun 2004, SAR interferograms 1–2) and Fig. 15b (from 31 Oct 2004 to 20

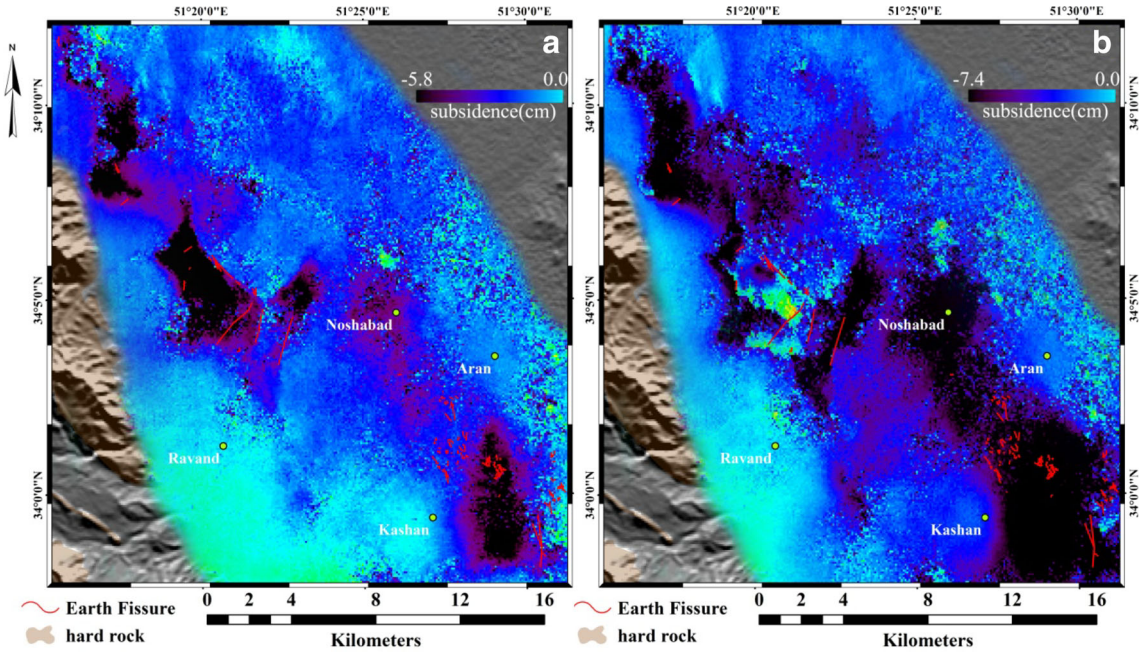

Fig. 15 Relation between the location of earth fissures and subsidence zones, Fig. 15a (from 12 Oct 2003 to 13 Jun 2004, SAR interferograms 1–2) and Fig. 15b (from 31 Oct 2004 to 20 Nov 2005, SAR interferograms 4–8)

Nov 2005, SAR interferograms 4–8). According to Fig. 15a, the earth fissures are formed north of Ravand at the boundary of the subsidence zone, where tensile strains are at a maximum. Also shown in Fig. 15b, similar mechanisms occur between Kashan and Aran and east of Kashan.

Conclusion

Based on the obtained results, the main cause of ground subsidence in Kashan Plain is the decline in groundwater head, which is the result of an increase in number of deep wells and over pumping of groundwater. The maximum decline in groundwater head is observed north of Ravand (west of the plain) and east of Kashan City. The average rate of decline in groundwater head in Kashan Plain is about 0.58 m/year.

Geophysical studies indicate that the bedrock is not uniform, and in some areas, such as east of Kashan City, it is bowl-like, which has caused some changes in thickness of the aquifer.

The maximum rate of subsidence east of Kashan City, as determined by InSAR and time-series analysis, is about 3.5 cm/year.

The maximum thickness of compressible sediments and maximum decline in groundwater head are the major factors that control maximum rate of subsidence in the area. As a result of groundwater withdrawal and differential vertical compaction in the bowl-like part of the bedrock, the fissures are formed at the ground surface.

The results also indicate that there is good correlation between subsidence areas and areas with higher thickness of compressible sediments such as silts and clay, and in these areas, should be avoided for urban developments.

Acknowledgments This work was conducted in the framework of the subsidence project supported by the Isfahan Department of Regional Water, the Geological Survey of Iran (GSI) and the University of Isfahan. The authors would like to thank the European Space Agency (ESA) for providing SAR images (ENVISAT data).

References

Adrian OG, Rudolph DL, Cherry JA (1999) The analysis of long termland subsidence near Mexico City: field investigations and predictive modeling. Water Resour Res 35:3327–3341

Amelung F, Galloway DL, Bell JW, Zebker HA, Laczniak RJ (1999) Sensing the ups and downs of Las Vegas InSAR reveals structural control of land subsidence and aquifer-system deformation. Geology 27:483–486

Bates RL, Jackson JA (1980) Glossary of geology, 2nd edn. American Geological Institute, Falls Church

Bell FG (1999) Geological hazards: their assessment, avoidance and mitigation. Routledge, New York

Bell JW, Amelung F, Ramelli AR, Blewitt G (2002) Land subsidence in Las Vegas, Nevada, 1935–2000: new geodetic data show evolution, revised spatial patterns, and reduced rates. Geosci Eng Geosci VIII(3):155–174

Berardino P, Fornaro G, Lanari R, Sansosti E (2002) A new algorithm for surface deformation monitoring based on small baseline

differential SAR interferograms. IEEE Trans Geosci Remote Sens 40:2375–2383
Boni R, Herrera G, Meisina C, Notti D, Bejar-Pizarro M, Zucca F, Gonzalez PJ, Palano M, Tomas R, Fernandez J, Fernandez-Merodo JA, Mulas J, Aragon R, Guardiola-Albert C, Mora O (2015) Twenty-year advanced DInSAR analysis of severe land subsidence: the Alto Guadalentín Basin (Spain) case study. Eng Geo 198:40–52
Bouwer H (1977) Land subsidence and cracking due to groundwater depletion. Ground Water 15(5):358–364. doi:10.1111/j.1745-6584.1977.tb03180.x
Burbey TJ (2002) The influences of faults in basin fill deposits on land subsidence: Las Vegas valley, Nevada, USA. Hydrogeol J 10(5):525–538
Ezquerro P, Herrera G, Marchamalo M, Tomás R, Béjar-Pizarro M, Martínez R (2014) Aquasi-elastic aquifer deformational behavior: Madrid aquifer case study. J Hydrol 519:1192–1204
Farr T, Kobrick M (2000) Shuttle radar topography mission produces a wealth of data, Eos Trans. Am Geophys Union 81:583–585
Feth JH (1951) Structural reconnaissance of the Red Rock quadrangle. US Geol. Survey Open-File Report, Arizona, p 32
Freyre DC, Cerca M, Marin MH (2003) Propagation of fracturing related to land subsidence in the valley of Queretaro, Mexico. Multidisciplinary studies of land subsidence and regional fracturing in Fluvio-Lacustrin Basons: 3 April 2003: Puerto Vallarta, Mexico, p 12
Galloway DL, Burbey TJ (2011) Review: regional land subsidence accompanying groundwater extraction. Hydrogeol J 19(8):1459–1486
Gambolati G, Gatto P, Freeze A (1974) Predictive simulation of the subsidence of Venice. Science 183(4127):849–851
Goldstein RM, Werner C (1998) Radar interferograms filtering for geophysical applications. Geophys Res Lett 25(21):4035–4038
Helm DC (1994) Horizontal aquifer movement in a Theis-Thiem confined system. Water Resour Res 30(4):953–964
Herrera G, Fernandez R, Tomas G, Cooksley MJ (2009) Advanced interpretation of subsidence in Murcia (SE Spain) using A-DInSAR data—modelling and validation. Nat Hazards Earth Syst Sci 9:647–661
Hoffmann J, Zebker HA, Galloway DL, Amelung F (2001) Seasonal subsidence and rebound in Las Vegas Valley, Nevada, observed by synthetic aperture radar interferometry. Water Resour Res 37:1551–1566
Holzer TL, Pampeyan EH (1981) Earth fissures and localized differential subsidence. Water Resour Res 17(1):223–227
Jachens RC, Holzer TL (1979) Geophysical investigations of ground failure to groundwater withdrawal, Picacho basin, Arizona. Ground Water 17(6):574–585
Jachens RC, Holzer TL (1982) Differential compaction mechanism for earth fissures near Casa Grande, Arizona. Geo Soc Am Bull 93:998–1012
Kontogianni V, Pytharouli S, Stiros S (2007) Ground subsidence, Quaternary faults and vulnerability of utilities and transportation networks in Thessaly, Greece. Environ Geol 52:1085–1095
Donglie L, Yunfeng S, Zhenguo L, Björn R, Sowter A, Wolfgang N, Zhengfu B (2014) Evaluation of InSAR and TomoSAR for monitoring deformations caused by mining in a mountainous area with high resolution satellite-based SAR. Remote Sens 6:1476–1495. doi:10.3390/rs6021476
Lofgren BE (1978) Hydraulic stresses cause ground movement and fissures, Picacho, Arizona. Geo Soc Am Abstr Programs 10(3):113
Massonnet D, Feigl KL (1998) Radar interferometry and its application to changes in the earth's surface. Rev Geophy 36(4):441–500
Motagh M, Walter RT, Sharifi MA, Fielding E, Schenk A, Andersohn J, Zschau J (2008) Land subsidence in Iran caused by widespread water reservoir over exploitation. Geophys Res Lett 35(16):403–412
Mousavi SM, Shamsai A, Naggar MHE, Khamehchian M (2001) A GPS-based monitoring program of land subsidence due to groundwater withdrawal in Iran. Can J Civ Eng 28(3):452–464
Phien-wej N, Giao PH, Nutalaya P (2006) Land subsidence in Bangkok, Thailand. Eng Geol 82(4):187–201
Raucoules D, Colesanti C, Carnec C (2007) Use of SAR interferometry for detecting and assessing ground subsidence. Comptes Rendus Geosci 339:289–302
Rojas E, Arzate J, Arroyo M (2002) A method to predict the group fissuring and faulting caused by regional groundwater decline. Eng Geol 65:245–260
Saracin A, Cosarca C, Didulescu C, Savu A, Nwgrila A (2014) Using InSAR technology for monitoring vertical deformation of the earth surface. Advances in environmental development, geomatics engineering and tourism. Proceedings of the 2nd European conference of geodesy & geomatics engineering (GENG '14), Brasov, Romania, June 26–28, 2014, p 41–48
Schmidt DA, Burgmann R (2003) Time dependent land uplift and subsidence in the Santa Clara valley, California, from a large InSAR data set. J Geophys Res. doi:10.1029/2002JB002267
Schumann HH, Cripe LS (1986) Land subsidence and earth fissures caused by groundwater depletion in Southern Arizona, USA. In: Johnson AI, Carbognin L, Ubertini L (eds), Proceedings of the 3rd international symposium on land subsidence, Venice, Italy, 19–25 March 1984, p 841–851, International Association of Hydrological Sciences (Publication 151)
Sheng Z, Helm DC, Jiang L (2003) Mechanisms of earth fissuring caused by groundwater withdrawal. Environ Eng Geosci 9(4):351–362
Slaff S (1993) Land subsidence and earth fissures in Arizona, down-to-earth series, Ariz Geol Surv: p 22
Trinh MT, Fredlund DG (2000) Modelling subsidence in the Hanoi City area, Vietnam. J Can Geotech 37:621–637
Waltham AC (1989) Ground subsidence. Chapman and Hall, New York
Wang GY, You G, Shi B, Yu J, Tuck M (2009) Long-term land subsidence and strata compression in Changzhou, China. Eng Geol 104:109–118
Werner C, Wegmuller U, Strozzi T, Weismann A (2000) Gamma SAR and interferometric processing software. Proceedings of the ERS-Envisat symposium, gothenburg, Sweden